New Structure in the Shapley Supercluster

M. J. Drinkwater[1], D. Proust[2], Q. A. Parker[3],
H. Quintana[4] and E. Slezak[5]

[1]School of Physics, University of New South Wales, Sydney, NSW 2052, Australia
Present address: School of Physics, University of Melbourne,
Parkville, Vic. 3052, Australia
m.drinkwater@physics.unimelb.edu.au
[2]DAEC, Observatoire de Meudon, 92195 Meudon Cedex, France
[3]Anglo-Australian Observatory, Coonabarabran, NSW 2357, Australia
Present address: Royal Observatory Edinburgh, Blackford Hill,
Edinburgh, EH9 3HJ, UK
qap@rpe.ac.UK
[4]Departamento de Astronomia y Astrofisica, Pontificia Universidad Católica de Chile,
Casilla 104, Santiago 22, Chile
hquintana@astro.puc.cl
[5]Observatoire de Nice, 06304 Nice, Cedex 4, France
slezak@obs-nice.fr

Abstract: We present new radial velocities for 306 bright ($R < 16$) galaxies in a 77 deg^2 region of the Shapley supercluster, measured with the FLAIR-II spectrograph on the UK Schmidt Telescope. The galaxies we measured were uniformly distributed over the survey area, in contrast to previous samples which were concentrated in several rich Abell clusters. Most of the galaxies (230) were members of the Shapley supercluster: they trace out two previously unknown sheets of galaxies linking the Abell clusters of the supercluster. In a 44 deg^2 area of the supercluster excluding the Abell clusters, these sheets alone represent an overdensity of a factor of $2 \cdot 0 \pm 0 \cdot 2$ compared to a uniform galaxy distribution. The supercluster is not flattened in the Declination direction as has been suggested in previous papers. Within our survey area the new galaxies contribute an additional 50% to the known contents of the Shapley supercluster, with a corresponding increase in its contribution to the motion of the Local Group.

Keywords: galaxies: clusters, distances and redshifts — large-scale structure of universe

1 Introduction

The Shapley supercluster (SSC) has been investigated by numerous authors since its discovery in 1930 (Quintana et al. 1995, hereafter Paper I). It lies in the general direction of the dipole anisotropy of the Cosmic Microwave Background (CMB), and is located at 130 h_{75}^{-1} Mpc beyond the Hydra-Centaurus supercluster ($\simeq 50$ h_{75}^{-1} Mpc away from us). It consists of many clusters and groups of galaxies in the redshift range $0 \cdot 04 < z < 0 \cdot 055$. The central cluster A3558 has also been measured with a ROSAT PSPC observation by Bardelli et al. (1996), who derived a total mass of $M_{tot} = 3 \cdot 1 \times 10^{14}$ $M_{\odot}$ within an Abell radius of 2 h_{75}^{-1} Mpc. Several other X-ray clusters form part of the Shapley supercluster (Pierre et al. 1994).

The Shapley supercluster is recognised as one of the most massive concentrations of galaxies in the local universe (Scaramella et al. 1989; Raychaudhury 1989), so it is of particular interest to consider its effect on the dynamics of the Local Group. In Paper I it was estimated that for $\Omega_0 = 0 \cdot 3$ and $H_0 = 75$ km s^{-1}Mpc^{-1} the gravitational pull of the supercluster may account for up to 25% of the peculiar velocity of the Local Group required to explain the dipole anisotropy of the CMB radiation, in which case the mass of the supercluster would be dominated by intercluster dark matter.

Previous studies of the Shapley supercluster (Paper I; Quintana et al. 1997, hereafter Paper II) have concentrated on the various rich Abell galaxy clusters in the region, but this might give a very biased view of the supercluster. As was noted in Paper I, 'the galaxy distribution inside the supercluster must be confirmed by the detection in redshift space of bridges or clouds of galaxies connecting the different clusters'.

We are continuing this project, using data from wide-field multi-fibre spectrographs to measure many more galaxy redshifts and get a more complete picture of the composition of the supercluster. Our main aims are first to define the real topology of the SSC (in Paper I it was shown that the SSC is significantly flattened, but the real extent of the concentration is not well defined) and second to analyse the individual X-ray clusters that are true members of the Shapley Supercluster, in order to estimate the cluster masses and investigate suspected substructure. Additional observations are planned before we present a full analysis of the dynamics (Proust et al. 1999, in preparation).

In Paper II we presented data from the MEFOS spectrograph on the European Southern Observatory 3·60 m telescope. This has 30 fibres in a 1 deg diameter field, so the observations were again mainly concentrated on the known clusters, determining for several of them whether they were members of the supercluster or not.

In this paper we present new data obtained with the FLAIR-II (Parker & Watson 1995; Parker 1997) multi-fibre spectrograph on the UK Schmidt Telescope at the Anglo-Australian Observatory. This has 90 fibres in a $5·5 \times 5·5$ deg^2 field and has allowed us to measure a much more uniform distribution of galaxies in the direction of the SSC, avoiding the previous bias in favour of the rich clusters. Our data reveal the existence of a sheet of galaxies connecting the main parts of the supercluster. We describe the sample and observations in Section 2. We present the results along with previous measurements in Section 3 and discuss the significance of the measurements in Section 4.

2 Observations

Although a large body of galaxy velocity data is available in the literature for the SSC, the existing samples of redshifts in each cluster are highly incomplete, even at the bright end of the luminosity function. We have therefore started a campaign to obtain complete samples down to the same magnitude below L_* for each cluster. Each selected cluster has a projected diameter of 2·5 to 3·0 degrees, so the FLAIR-II system on the UKST, with its $5·5 \times 5·5$ deg^2 field, is an ideal facility for this project. The very wide field also permits us to probe the regions between the dominant clusters

that have been neglected in previous observations. In this paper we emphasise our results from these regions.

We selected targets from red ESO/SRC sky survey plates scanned by the MAMA machine at Paris Observatory (as described in Paper II; see also Infante, Slezak & Quintana 1996). The fields observed (listed in Table 1) were the standard survey fields nearest to the centre of the cluster (13:25:00, -31:00:00 B1950). These covered an area of 77 deg^2, allowing us to probe the limits of the SSC out to radii as large as 8 deg.

We defined a sample of galaxies to a limit of $R < 16$, corresponding (assuming a mean $B - R = 1·5$) to $B < 17·5$, the nominal galaxy limiting magnitude of the FLAIR-II system. This corresponds to an absolute magnitude of $M_B = -19$ at the Shapley distance of 200 h$_{75}^{-1}$ Mpc. This gave samples of 600–1000 galaxies per field. We then removed any galaxies with published measurements in the NED database or measured by H. Quintana and R. Carrasco (private communication, 1997): 46 galaxies for F382, 81 for F383 and 200 for F444. For each observing run we then selected random subsamples of about 110 targets per field from the unobserved galaxies. When preparing each field for observation at the telescope, we made a further selection of 80 targets to observe (10 fibres being reserved for measurement of the sky background). This final selection was essentially random, but we did reject any galaxies too close (less than about 1 arcminute) to another target already chosen or a bright star.

We observed a total of 3 fields with the FLAIR-II spectrograph in 1997 May and two more in 1998 April. The details of the observations are given in Table 1. In 1997, out of 6 allocated nights, we were only able to observe 3 FLAIR fields successfully due to poor weather and the first of these was repeated over 3 nights. Field F444 was observed in particularly poor weather, resulting in a much lower number of measured redshifts. In 1998 we again had poor weather, and were only able to observe two fields in an allocation of 8 half-nights.

The data were reduced as described in Drinkwater et al. (1996), using the dofibers package in IRAF (Tody 1993). We measured the radial velocities with the RVSAO package (Kurtz & Mink 1998) contributed to IRAF.

Table 1.   Journal of FLAIR observations

Date	Field	RA (1950)	Dec	Exposure	Seeing	Weather	N_z
1997 May 5	F382	13:12:00	-35:00:00	18 000s	2–3$''$	cloud	69
1997 May 6	F444	13:25:00	-30:00:00	15 000s	2–3$''$	cloud	47
1997 May 8	F383	13:36:00	-35:00:00	18 000s	3–5$''$	clear	73
1998 April 25	F383	13:36:00	-35:00:00	15 000s	2–3$''$	clear	61
1998 April 27	F382	13:12:00	-35:00:00	21 000s	3–5$''$	cloud	56

Note: N_z is the number of galaxies with measured redshifts in each field.

Table 2. Galaxies observed

RA (B1950) Dec	Field	m_R	V (km s^{-1})	σ_V	RA (B1950) Dec	Field	m_R	V (km s^{-1})	σ_V
13:00:14·3 −36:21:34	382	15·86	3443	36	13:10:54·7 −35:10:08	382	14·99	7527	96
13:00:35·5 −33:42:37	382	15·53	23713	68	13:11:02·1 −36:16:46	382	14·52	14367	76
13:01:07·2 −36:16:08	382	14·32	10298	56	13:11:09·8 −33:39:12	382	14·21	15299	49
13:01:28·5 −36:11:57	382	15·74	27469	33	13:11:22·4 −33:49:50	382	14·63	15355	81
13:01:30·0 −33:36:27	382	15·80	21437	126	13:11:23·5 −36:57:36	382	15·21	10229	83
13:01:34·5 −37:14:51	382	15·61	15818	101	13:11:30·6 −36:55:53	382	14·26	10688	59
13:02:11·4 −36:34:14	382	15·84	17698	13	13:11:42·3 −33:07:11	382	14·46	8889	69
13:02:38·8 −36:15:49	382	14·90	37525	71	13:11:54·3 −33:05:46	382	15·58	14649	115
13:02:50·6 −34:01:55	382	15·86	25647	42	13:12:05·7 −33:29:36	382	15·99	30594	115
13:03:01·9 −36:28:58	382	14·39	10092	72	13:12:19·3 −32:37:16	382	15·51	14280	90
13:03:14·3 −37:20:00	382	15·50	14899	97	13:12:23·9 −33:22:29	382	14·20	14531	79
13:03:16·0 −35:44:30	382	15·70	24066	96	13:12:39·3 −36:55:29	382	15·66	10048	85
13:03:28·1 −36:44:17	382	15·65	14943	69	13:12:39·9 −32:26:47	444	14·15	13869	96
13:03:44·6 −35:40:23	382	15·78	14737	72	13:13:13·3 −36:43:06	382	15·90	31971	88
13:03:48·0 −33:55:36	382	15·62	25475	184	13:13:21·9 −32:37:24	382	14·71	15284	88
13:04:03·2 −36:42:55	382	15·92	15011	215	13:13:34·6 −35:00:24	382	15·81	11473	98
13:04:08·4 −37:06:37	382	15·65	14058	47	13:13:37·9 −32:35:56	382	15·92	14428	86
13:04:32·6 −35:51:35	382	14·53	15099	75	13:13:40·5 −37:12:41	382	15·45	14637	23
13:04:46·9 −32:34:17	382	14·24	15419	132	13:13:54·9 −32:59:57	382	15·08	14315	98
13:04:49·9 −34:09:57	382	15·97	18872	37	13:13:59·8 −35:31:47	382	15·80	32384	102
13:04:56·2 −37:19:11	382	15·31	15024	60	13:14:30·4 −31:33:07	444	15·97	14998	126
13:05:12·2 −37:06:25	382	15·48	13228	117	13:14:35·9 −33:11:02	382	14·26	15334	48
13:05:19·9 −33:00:31	382	15·64	10171	150	13:14:37·9 −33:39:08	382	14·86	15224	73
13:05:20·7 −34:03:32	382	15·69	15174	163	13:14:44·4 −31:20:39	444	15·83	15632	176
13:05:23·1 −35:56:31	382	15·87	15763	139	13:15:00·6 −32:57:45	382	15·93	25689	64
13:05:40·8 −34:09:29	382	15·19	15067	78	13:15:08·7 −37:10:05	382	14·68	7330	66
13:06:10·3 −37:15:19	382	15·90	14312	81	13:15:17·0 −35:32:43	382	14·98	3265	94
13:06:34·7 −34:29:38	382	15·21	13201	76	13:15:18·1 −29:53:31	444	15·34	9769	73
13:06:47·3 −34:25:01	382	15·91	18578	77	13:15:18·6 −36:43:14	382	15·30	14921	28
13:06:55·9 −35:20:35	382	15·40	28284	52	13:15:21·3 −31:45:59	444	14·64	4358	114
13:07:07·2 −36:52:20	382	15·96	14350	61	13:15:29·4 −37:02:54	382	15·06	15014	63
13:07:29·6 −32:36:43	382	14·51	9507	81	13:15:38·5 −33:02:17	382	14·33	4342	51
13:07:34·8 −34:20:49	382	15·77	27522	60	13:16:06·6 −33:09:45	382	15·55	13407	47
13:07:48·3 −37:02:06	382	14·28	14555	42	13:16:07·8 −31:33:17	444	14·20	15641	103
13:08:01·8 −33:42:02	382	15·72	15113	95	13:16:17·3 −36:58:20	382	14·91	14311	86
13:08:19·8 −32:43:36	382	15·87	43801	44	13:16:31·5 −33:02:46	382	15·99	15047	69
13:08:20·1 −32:49:07	382	14·39	15899	84	13:16:38·9 −33:05:31	382	15·94	14960	70
13:08:25·4 −36:24:37	382	15·11	3363	89	13:16:38·9 −33:05:31	382	14·48	1247	28
13:08:27·2 −33:49:39	382	15·72	14837	25	13:16:40·8 −33:15:18	382	14·33	14981	98
13:09:01·9 −34:02:24	382	15·82	27235	66	13:16:41·2 −33:39:11	382	15·17	8432	37
13:09:07·1 −35:47:53	382	14·24	10491	54	13:16:49·5 −36:42:34	382	15·76	11687	66
13:09:15·4 −37:11:40	382	15·59	13069	119	13:17:08·9 −34:02:03	382	15·43	23525	110
13:09:19·3 −34:19:50	382	14·92	3196	80	13:17:24·0 −34:50:33	382	15·64	13924	121
13:09:34·3 −35:04:41	382	15·83	23360	77	13:17:28·8 −36:49:52	382	15·16	2359	47
13:09:35·1 −37:04:57	382	15·96	10414	81	13:17:38·4 −34:04:01	382	15·70	15106	145
13:09:39·0 −33:45:40	382	15·55	13063	141	13:17:47·5 −33:52:14	382	15·72	23532	69
13:09:53·9 −33:06:23	382	15·75	23141	79	13:17:53·0 −34:40:14	382	15·73	15393	86
13:09:55·1 −35:59:01	382	15·04	14386	63	13:18:05·5 −37:00:34	382	15·90	15980	78
13:10:13·6 −34:30:54	382	15·60	15159	154	13:18:06·6 −27:47:20	444	15·97	15326	122
13:10:31·9 −32:40:51	382	15·75	29991	72	13:18:15·6 −32:47:18	382	15·23	15768	64
13:10:47·9 −33:06:26	382	15·99	29645	117	13:18:16·1 −35:20:17	382	15·47	15654	85

Table 2 (*continued*)

RA (B1950) Dec	Field	m_R	V (km s^{-1})	σ_V	RA (B1950) Dec	Field	m_R	V (km s^{-1})	σ_V
13:18:26·7 −34:55:52	382	15·19	20402	58	13:25:41·9 −33:44:20	383	15·86	24911	114
13:18:31·3 −35:33:05	382	15·42	15373	163	13:25:42·1 −33:56:52	383	15·88	14661	129
13:18:36·3 −32:30:51	444	14·59	14469	110	13:26:14·4 −28:34:52	444	14·20	12289	58
13:18:38·8 −35:54:22	382	15·02	15345	94	13:26:27·7 −31:47:04	444	14·74	14060	114
13:18:50·7 −34:40:34	382	15·19	15222	196	13:26:39·2 −31:17:35	444	14·03	15430	87
13:18:58·0 −35:16:37	382	14·53	13903	170	13:26:52·9 −28:00:28	444	14·44	10015	119
13:19:01·6 −33:36:49	382	15·83	35049	132	13:27:09·0 −28:59:02	444	15·83	14201	114
13:19:07·6 −35:29:36	382	15·62	16535	91	13:27:14·2 −27:43:01	444	15·12	10237	114
13:19:15·1 −28:06:35	444	14·58	14030	85	13:27:22·6 −32:32:55	383	14·33	15666	78
13:19:21·1 −34:32:11	382	15·54	15664	126	13:27:24·1 −29:14:38	444	15·23	14488	30
13:19:26·8 −34:21:31	382	15·59	15667	127	13:27:39·0 −34:21:48	383	15·95	21467	84
13:19:39·1 −33:06:29	382	15·88	3497	96	13:27:51·3 −31:36:28	444	15·96	14470	75
13:19:47·9 −35:36:32	382	15·50	14747	142	13:28:11·4 −32:21:51	383	15·68	15986	64
13:19:54·1 −33:10:27	382	14·26	14379	44	13:28:19·5 −32:28:46	383	15·73	3468	95
13:20:04·8 −34:47:15	382	14·97	7237	96	13:28:32·5 −33:38:26	383	15·58	22089	90
13:20:10·1 −32:27:07	382	14·78	8503	67	13:28:58·4 −36:41:55	383	15·35	14996	97
13:20:13·1 −34:43:27	382	15·00	16498	84	13:29:07·6 −36:03:10	383	15·33	20314	76
13:20:24·0 −35:03:57	382	15·76	14710	59	13:29:14·5 −33:31:57	383	14·93	8770	66
13:20:52·7 −35:38:04	382	14·80	3792	78	13:29:16·4 −33:03:38	383	15·08	13640	98
13:20:53·3 −34:11:58	382	15·45	15426	126	13:29:24·5 −33:07:15	383	14·71	15243	81
13:20:57·0 −31:26:49	444	15·92	15170	63	13:29:33·4 −32:58:55	383	14·95	13916	47
13:20:58·5 −27:43:52	444	14·54	13674	69	13:29:33·7 −37:15:24	383	14·96	15295	29
13:21:04·1 −34:24:00	382	14·49	14472	103	13:29:40·1 −33:54:18	383	15·87	14770	96
13:21:05·8 −31:55:18	444	14·91	15249	107	13:29:40·9 −37:02:12	383	15·58	15687	101
13:21:08·5 −29:02:44	444	15·63	14096	98	13:29:49·3 −34:53:51	383	15·23	15122	39
13:21:30·5 −31:23:03	444	14·66	14390	176	13:30:00·5 −34:27:42	383	15·47	36879	77
13:21:33·1 −32:37:59	382	14·36	14251	135	13:30:00·7 −28:45:40	444	15·57	5526	93
13:21:37·9 −29:59:26	444	14·43	3634	98	13:30:04·4 −32:54:49	383	15·19	15698	50
13:21:39·8 −33:42:58	382	15·35	14827	87	13:30:10·9 −32:50:38	383	14·62	14951	53
13:21:51·8 −36:02:13	382	15·14	10771	96	13:30:13·4 −37:14:36	383	15·79	15164	67
13:21:58·5 −34:06:56	382	15·04	8371	106	13:30:14·9 −33:02:41	383	15·65	14838	115
13:22:02·2 −31:18:01	444	16·00	14773	14	13:30:15·5 −34:11:36	383	14·84	7491	16
13:22:20·4 −33:39:05	382	15·94	27194	132	13:30:19·9 −31:20:49	444	15·96	14559	123
13:22:46·5 −36:19:44	382	15·34	15208	42	13:30:34·1 −33:41:34	383	15·99	22010	143
13:22:56·5 −37:01:27	382	15·44	10225	123	13:30:45·7 −31:13:03	444	14·97	15201	74
13:23:22·9 −36:47:09	382	15·98	19958	150	13:30:53·3 −35:08:58	383	15·92	15377	147
13:23:57·5 −31:16:09	444	16·00	14660	117	13:31:01·2 −35:07:39	383	15·88	21640	89
13:24:04·7 −33:55:06	382	15·89	14909	34	13:31:17·6 −31:13:59	444	15·86	14842	89
13:24:08·5 −31:56:19	444	15·71	13839	84	13:31:17·8 −27:54:11	444	14·85	9187	74
13:24:12·5 −29:48:56	444	14·88	1866	78	13:31:19·5 −34:48:41	383	15·28	14917	69
13:24:15·0 −30:57:58	444	14·92	16332	122	13:31:21·8 −32:43:17	383	14·43	15177	70
13:24:18·1 −36:49:27	382	15·72	14367	76	13:31:25·2 −29:07:15	444	15·35	14008	96
13:24:21·4 −37:00:34	382	15·62	14520	36	13:31:30·3 −35:09:30	383	15·37	9416	65
13:24:28·2 −36:49:27	383	15·74	15098	102	13:31:33·2 −31:28:46	444	14·89	16271	85
13:24:28·4 −36:14:05	383	15·31	14658	62	13:31:39·7 −36:33:12	383	16·00	15274	150
13:24:35·3 −32:02:27	444	15·48	14176	82	13:31:48·9 −34:46:49	383	15·55	2367	21
13:24:58·9 −32:21:44	383	15·66	11832	16	13:31:53·3 −34:58:33	383	15·35	16579	20
13:25:13·1 −31:30:38	444	15·97	15590	96	13:32:17·4 −33:46:46	383	14·98	3878	52
13:25:14·4 −32:30:11	383	15·86	11585	57	13:32:28·5 −31:10:15	444	14·86	14845	86
13:25:20·1 −31:25:21	444	15·17	12200	135	13:32:31·3 −33:54:20	383	14·18	7208	66
13:25:25·0 −29:59:01	444	15·17	12776	81	13:32:48·9 −31:27:42	444	15·94	11794	98

Table 2 (*continued*)

RA (B1950) Dec	Field	m_R	V (km s^{-1})	σ_V	RA (B1950) Dec	Field	m_R	V (km s^{-1})	σ_V
13:32:54·0 −35:18:55	383	14·42	15438	54	13:40:33·4 −32:59:43	383	15·55	12267	97
13:33:21·5 −36:38:27	383	15·17	15135	51	13:40:34·0 −37:23:43	383	15·64	11113	52
13:33:37·8 −32:50:15	383	15·46	15688	105	13:40:40·2 −34:31:47	383	15·08	17030	72
13:33:41·2 −33:49:11	383	14·19	3787	43	13:40:42·0 −36:09:58	383	14·60	4311	59
13:33:45·9 −28:50:04	444	14·16	4516	89	13:40:52·6 −34:49:27	383	14·32	16227	183
13:34:05·6 −34:08:42	383	15·14	4133	76	13:40:59·8 −35:31:12	383	14·38	11637	28
13:34:11·1 −33:34:08	383	14·29	13931	87	13:41:14·7 −34:05:19	383	14·87	11202	76
13:34:12·6 −28:16:45	444	15·90	15262	98	13:41:23·2 −36:22:42	383	15·81	11498	46
13:34:28·4 −34:38:09	383	15·50	29247	103	13:41:23·9 −33:51:28	383	15·21	11818	71
13:34:43·7 −31:37:28	444	15·38	11598	98	13:41:47·3 −32:24:12	383	15·53	12438	76
13:34:45·1 −34:16:42	383	15·67	22108	68	13:41:49·3 −35:11:00	383	15·45	37694	72
13:34:49·6 −33:35:55	383	15·54	11289	85	13:41:52·3 −33:21:05	383	14·32	11063	31
13:34:50·2 −35:14:29	383	16·00	15162	89	13:41:55·5 −34:22:45	383	15·24	14660	48
13:34:59·3 −35:23:12	383	14·68	15695	71	13:42:08·6 −34:58:58	383	15·67	17045	66
13:35:15·2 −34:48:29	383	15·47	15162	92	13:42:10·1 −32:38:25	383	15·77	12085	83
13:35:21·3 −31:41:48	444	15·26	14694	127	13:42:25·1 −32:23:47	383	14·23	9469	41
13:35:27·8 −35:42:28	383	15·50	11327	74	13:42:33·6 −36:31:58	383	15·05	11531	64
13:35:47·0 −34:17:07	383	15·24	15420	116	13:42:38·9 −35:01:09	383	15·79	17237	50
13:35:52·1 −35:13:11	383	15·91	14685	37	13:42:56·1 −33:46:54	383	15·10	15058	33
13:36:00·6 −36:11:38	383	14·66	13789	55	13:43:08·2 −33:29:39	383	14·32	11662	44
13:36:04·4 −35:22:16	383	15·50	15223	89	13:43:17·6 −34:14:50	383	15·67	24806	35
13:36:04·7 −36:20:26	383	15·80	13755	74	13:43:29·2 −32:55:23	383	15·54	11760	52
13:36:08·6 −32:20:51	444	14·76	16298	77	13:43:32·6 −35:50:50	383	15·11	11548	27
13:36:15·9 −36:39:42	383	15·30	15741	44	13:43:33·0 −32:24:59	383	15·36	12884	52
13:36:18·3 −33:47:22	383	15·75	21245	28	13:44:02·0 −33:04:05	383	15·98	11113	157
13:36:32·6 −35:12:49	383	15·47	19147	68	13:44:06·5 −37:12:33	383	15·71	11357	50
13:36:43·3 −35:24:54	383	15·19	15791	78	13:44:06·7 −35:03:53	383	15·23	11453	47
13:36:44·2 −33:45:54	383	15·13	15268	76	13:44:15·6 −32:39:29	383	15·76	12304	159
13:36:49·8 −35:41:31	383	15·49	29346	77	13:44:16·1 −33:08:38	383	15·44	11518	77
13:36:56·1 −33:24:07	383	14·54	15381	43	13:44:19·6 −33:23:43	383	15·87	13010	70
13:36:56·6 −32:49:51	383	15·43	15345	135	13:44:22·8 −36:07:31	383	15·04	10963	66
13:37:12·1 −32:48:53	383	15·43	11841	59	13:44:29·3 −33:21:14	383	15·38	16117	48
13:37:14·8 −32:35:15	383	14·56	7254	14	13:44:29·5 −32:50:50	383	14·99	11694	49
13:37:15·1 −34:05:41	383	15·66	21441	89	13:44:56·8 −32:56:05	383	14·92	10328	29
13:37:37·8 −33:44:08	383	15·91	14867	61	13:45:05·5 −32:37:12	383	15·59	11789	80
13:37:39·9 −35:25:16	383	15·54	15641	57	13:45:11·0 −33:06:07	383	14·35	11901	34
13:37:59·8 −33:53:02	383	15·99	15579	30	13:45:18·8 −32:32:24	383	15·74	12585	138
13:38:01·9 −33:25:24	383	15·47	15167	66	13:45:29·9 −34:26:11	383	15·15	13896	88
13:38:12·4 −34:07:13	383	15·57	15485	98	13:45:37·7 −35:26:14	383	15·90	30107	78
13:38:22·3 −35:24:09	383	14·38	15068	85	13:45:47·9 −34:24:28	383	15·29	27740	73
13:38:39·8 −34:07:45	383	15·56	16973	66	13:45:49·1 −37:14:52	383	15·47	11128	83
13:38:40·8 −33:41:14	383	15·39	15161	48	13:46:04·9 −32:36:32	383	14·39	11603	49
13:38:49·2 −33:49:06	383	15·76	14610	47	13:46:05·4 −33:09:44	383	14·72	10868	31
13:38:52·4 −35:37:34	383	14·88	11378	62	13:46:06·3 −33:43:18	383	15·06	11327	35
13:38:57·2 −32:55:58	383	15·49	11945	65	13:46:56·0 −35:14:07	383	15·60	28576	122
13:39:27·0 −36:56:20	383	14·84	11288	31	13:46:59·9 −33:02:31	383	15·78	16129	67
13:39:35·6 −34:37:32	383	15·61	4454	51	13:47:03·7 −36:30:57	383	15·22	30091	89
13:39:43·7 −37:21:55	383	15·78	10122	76	13:47:22·5 −32:49:37	383	14·35	10522	50
13:39:55·3 −35:55:15	383	15·64	21887	155	13:47:38·1 −32:25:54	383	15·49	11098	51
13:40:02·0 −34:43:11	383	15·07	16170	50	13:47:48·9 −32:38:51	383	15·12	11270	37
13:40:26·8 −36:04:17	383	15·18	24883	122	13:48:08·4 −35:50:11	383	15·46	22610	95

Figure 1—Distribution of galaxies measured with FLAIR-II (squares) in the three UK Schmidt fields (large dashed squares) observed. The coordinate axes are for equinox B1950. Also shown are previously measured galaxies (dots) and known Abell clusters (labelled circles).

Figure 2—Cone diagrams of all known galaxy redshifts in the direction of the Shapley supercluster. Previously published galaxies are plotted as dots; the new measurements are plotted as open squares. The angular scale is enlarged by a factor of 3 for clarity. The distribution in Declination is repeated at the right for comparison without the new measurements.

Redshifts were measured for absorption-featured spectra using the cross-correlation task XCSAO in RVSAO. We decided to adopt as the absorption velocity the one associated with the minimum error from the cross-correlation against the templates. In the great majority of cases, this coincided also with the maximum R parameter of Tonry & Davis (1979). The redshifts for the emission-line objects were determined using the EMSAO task in RVSAO. EMSAO finds emission lines automatically, computes redshifts for each identified line and combines them into a single radial velocity with error. Spectra showing both absorption and emission features were generally measured with the two tasks XCSAO and EMSAO and the result with the lower error used. In two spectra with very poor signal $(13:05:19\cdot9, -33:00:31$ and $13:23:22\cdot9, -36:47:09)$ the emission lines were measured manually and a conservative error of 150 km s^{-1} assigned. We measured velocities successfully for 306 galaxies in the sample; these are presented in Table 2.

We have compared the distributions of the galaxies we measured to the input samples to check that they are fair samples. There is no significant difference in the distributions of the coordinates, but there is a small difference in the magnitude distributions in the sense that the measured sample does not have as many of the faintest galaxies as the input sample. This is to be expected, as these would have the lowest signal in the FLAIR-II spectra, but this should not affect our study of the spatial distribution significantly.

3 Results

Previous studies of the SSC have covered a very large region of sky, but we will limit our analysis in this paper to the region of sky we observed with FLAIR-II: the three UK Schmidt fields in Table 1. In some cases we will further restrict our analysis to the two southern fields F382 and F383, where our observations were much more complete. The distribution of these fields and the galaxies we observed is shown in Figure 1. We also show any previously observed galaxies and the known Abell clusters.

We present the resulting distribution of galaxies towards the SSC in Figure 2 as cone diagrams and in Figure 3 as the histogram of all velocities up to 40 000 km s^{-1}. The importance of the SSC in this region of the sky is demonstrated by the fact that fully-three quarters of the galaxies we measured belong to the SSC with velocities in the range 7580–18 300 km s^{-1}. In all the plots the new data are indicated by different symbols to emphasise their impact (this can also be seen by comparing these figures with the equivalent ones in Paper II). It can be seen that by probing large regions of the SSC away from the rich Abell clusters, we have revealed additional structures which we discuss in the following sections.
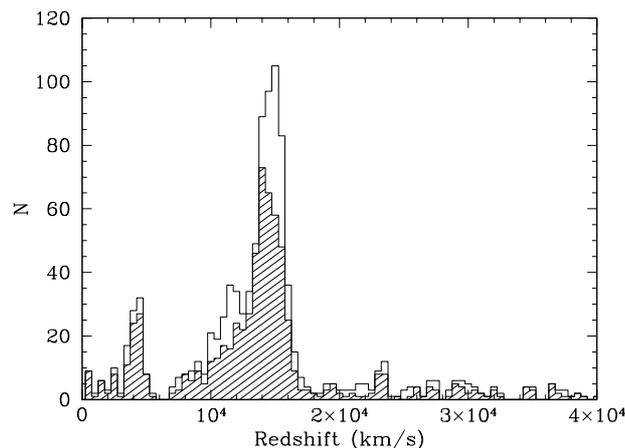

Figure 3—Histogram of galaxy redshifts in the direction of the Shapley supercluster in the region defined by the three Schmidt fields shown in Figure 1 with a step size of 500 km s^{-1}. The upper histogram is for all the data and the lower histogram gives just the previously published data.

3.1 Foreground Galaxies

First, in agreement with previous work, we note the presence of a foreground wall of 269 galaxies (Hydra–Centaurus region) at $\overline{V} = 4242$ km s^{-1} with $\sigma = 890$ km s^{-1} in the range 2000–6000 km s^{-1}. This distribution can be related with the nearby cluster A3627 associated with the 'Great Attractor' (Kraan-Korteweg et al. 1996).

3.2 Clusters in the Shapley Supercluster

The previous observations reported in Papers I and II concentrated on the Abell clusters, clarifying the locations of many of them. We reproduce a list of the main clusters in the SSC region in Table 3 for references and plot their positions in Figure 1. As noted above, our new measurements concentrate on galaxies outside the rich clusters in this field. In particular, we observed virtually no galaxies in foreground or background clusters. We compare the distribution of the SSC galaxies to that of the Abell clusters in two velocity slices in Figures 4 and 5.

In the near side of the SSC $(7580 < v < 12\,700$ km s^{-1} Figure 4) we detected several new galaxies in the clusters A3571 and A3572. This region has a very extended velocity structure with several galaxies in the higher range (Figure 5). At the velocity of the main part of the SSC $(12\,700 < v < 18\,300$ km s^{-1} Figure 5) we have found additional galaxies in many of the clusters, especially the poorer ones like AS726, AS731 and A3564. The main conclusion, however, is that the clusters are seen as peaks in a sheet-like distribution, rather than isolated objects.

3.3 Structure of the Shapley Supercluster

The main impact of our new data is an improvement in our knowledge of the large-scale structure of the SSC obtained through the measurement of a large
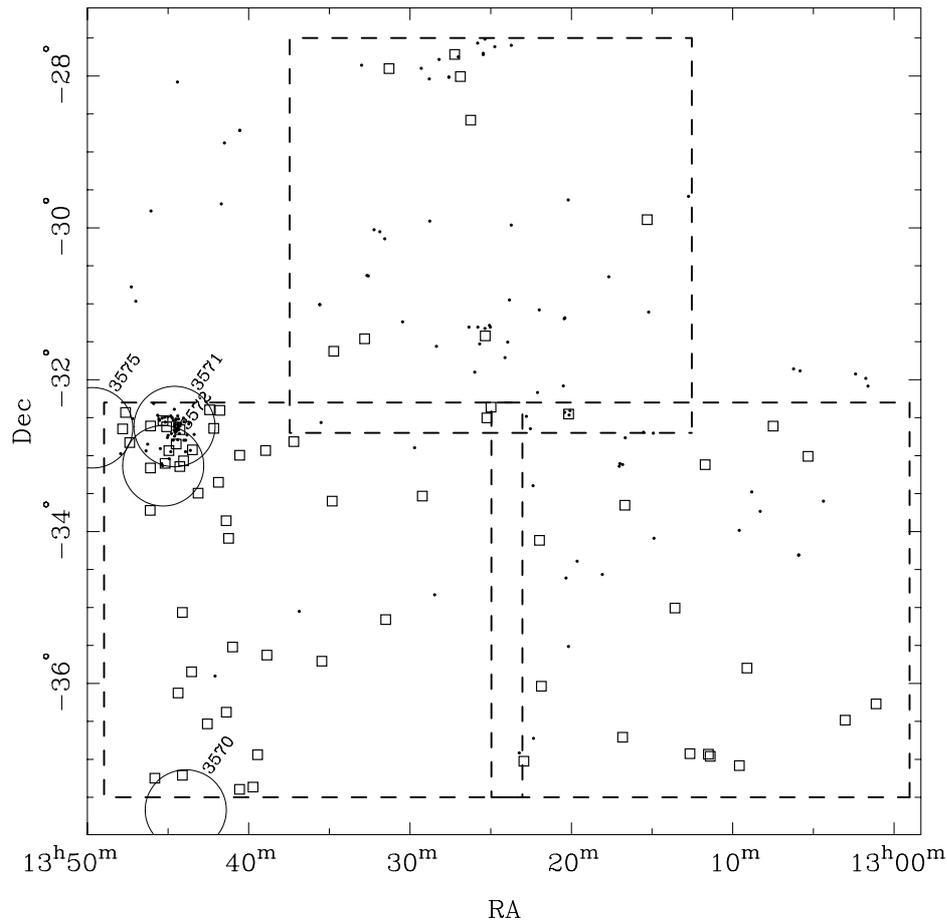
Figure 4—Galaxies and clusters in the direction of the Shapley supercluster with velocities in the range $7580 < v < 12\,700$ km s^{-1} (near side of the main supercluster). Previously reported galaxies are plotted as dots and our new measurements are plotted as open squares. Abell clusters in this velocity range are plotted as labelled circles of radius $0 \cdot 5$ deg (approximately 1 Abell radius at this distance).

number of galaxies away from the rich Abell clusters previously studied. The majority of the galaxies we observed were part of the SSC, so our principal result is that the SSC is bigger than previously thought, with an additional 230 galaxies in the velocity range $7580 < v < 18\,300$ km s^{-1} compared to 492 previously known in our survey area.

Looking at the cone diagrams (Figure 2) and the velocity histogram (Figure 3) our first new observation is that the SSC is clearly separated into two components in velocity space, the nearer one at $\overline{v} = 10\,800$ km s^{-1} ($\sigma_v = 1300$ km s^{-1}) to the East of the main concentration at $\overline{v} = 14\,920$ km s^{-1} ($\sigma_v = 1100$ km s^{-1}). The two regions contain 200 and 522 galaxies respectively. Some evidence for this separation was noted in the velocity distribution in Paper II, but it is much clearer our new data.

Secondly, it can be see from the Declination cone diagram in Figure 2 as well as the sky plots in Figures 4 and 5 that the southern part of the SSC consists of two large sheets of galaxies, of which the previously measured Abell clusters represent the peaks of maximum density.

To consider the significance of this extended distribution of galaxies, it is helpful to define an inter-cluster sample consisting of galaxies in the southern fields (F382 and F383) outside the known Abell clusters in the SSC velocity range. We eliminated all galaxies within a $0 \cdot 5$ degree radius (about 1 Abell radius) of all the clusters shown in Figures 4 and 5. Very few of the previously measured galaxies remain in the sample. In Figure 6 we plot a histogram of the galaxy velocities in this inter-cluster sample compared to the predicted $n(z)$ distribution of galaxies. The predicted distribution was based on the number counts of Metcalfe et al. (1991), normalised to the area of the southern sample after removing clusters (44 deg^2) and corrected for completeness (304 out of a possible 1194 galaxies measured in total). We also show the histogram (shaded) and predictions (dashed) for the previously measured galaxies in the same field (128 out of a possible 1194). The histogram shows that even for the inter-cluster galaxies there is a large overdensity in the SSC region ($7500 < cz < 18\,500$ km s^{-1}): we measure 161 galaxies compared to 74 expected. This is an overdensity of $2 \cdot 0 \pm 0 \cdot 2$ detected at the 10 sigma level. This is averaged over the whole SSC velocity range; the overdensity in individual 1000 km s^{-1} bins peaks at about 7. By comparison
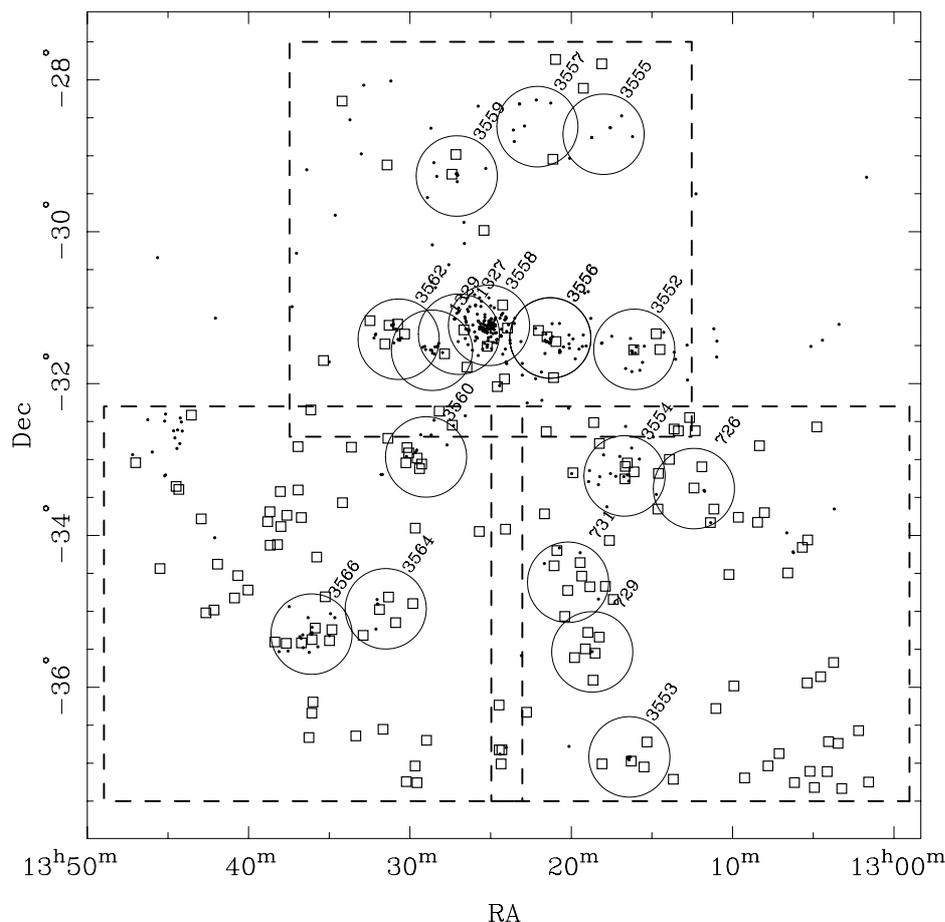
Figure 5—Galaxies and clusters in the direction of the Shapley supercluster with velocities in the range $12\,700 < v < 18\,300\ \mathrm{km\,s^{-1}}$ (main supercluster). Previously reported galaxies are plotted as dots and our new measurements are plotted as open squares. Abell clusters in this velocity range are plotted as labelled circles of radius $0\cdot5$ deg (approximately 1 Abell radius at this distance).
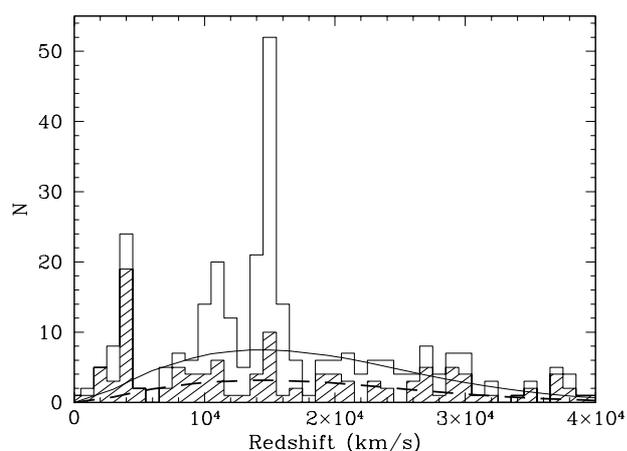

Figure 6—Histogram of all galaxy redshifts in southern inter-cluster region of the Shapley supercluster with a bin size of $1000\ \mathrm{km\,s^{-1}}$. The upper histogram is for both our new data and the previously published data; the lower histogram gives just the old data. For each histogram a curve shows the predicted distribution, allowing for the size of the region and the completeness of the samples based on a uniform galaxy distribution (Metcalfe et al. 1991).

the previous data (42 galaxies, 33 expected) gave an overdensity of $1\cdot3$ detected at only $1\cdot5\sigma$. The overdensity for the whole SSC including the Abell clusters is, of course, much larger still.

These new observations mean that we must modify the conclusions of Paper I about the overall shape of the SSC. In Paper I it was concluded from the velocity distribution of the clusters that the SSC was very elongated and either inclined towards us or rotating. The SSC extends as far as our measurements to the South, so we find it is not elongated or flattened. We now suggest that it is more complex still, being composed of the known Abell clusters embedded in two sheets of galaxies of much larger extent.

4 Discussion

Our new observations of galaxies towards the Shapely supercluster have, by surveying a large area away from known clusters, revealed substantial new large

Table 3. Abell clusters in the Shapley region

RA (B1950)	Dec.	cz (km s^{-1})	Name	Dist.	Ref.
12:47:12	−36:29:00	−	35276	6	N
12:51:18	−26:07:00	−	1633	6	N
12:51:36	−28:45:00	15 854	3528	4	I
12:52:54	−30:05:00	15 960	3530	4	I
12:54:24	−32:39:00	22 454	3531	5	II
12:54:36	−30:06:00	16 100	3532	4	I
12:56:18	−26:21:00	22 994	1648	−	N
12:57:00	−33:24:00	14 330	S718	4	II
12:58:18	−32:10:00	5 007	3537	−	N
13:05:54	−34:18:00	27 551	3542·1	4	II
13:05:54	−34:18:00	39 393	3542·2	4	II
13:08:36	−33:49:00	22 245	3545	6	II
13:11:36	−29:11:00	22 634	3549	5	II
13:12:24	−33:23:00	17 688	S726	5	I
13:16:06	−31:33:00	14 818	3552	6	I
13:16:24	−36:55:00	15 110	3553	4	I
13:16:42	−33:13:00	14 570	3554	4	II
13:18:00	−28:43:00	14 810	3555	4	I
13:18:42	−35:32:00	14 960	S729	5	I
13:20:12	−34:37:00	15 140	S731	4	II
13:21:18	−31:24:00	14 130	3556·1	4	B
13:21:18	−31:24:00	15 066	3556·2	4	B
13:22:06	−28:37:00	14 270	3557·1	5	II
13:22:06	−28:37:00	23 084	3557·2	5	II
13:23:00	−36:59:00	20 806	S733	-	N
13:24:06	−26:51:00	10 368	1736·1	3	I
13:24:06	−26:51:00	13 357	1736·2	3	I
13:25:06	−31:14:00	14 403	3558	3	B
13:26:58	−31:21:00	14 841	1327	-	N
13:27:06	−29:16:00	13 812	3559	4	I
13:28:38	−31:33:43	12 868	1329	-	I
13:29:00	−32:58:00	13 864	3560	3	I
13:30:42	−31:25:00	14 492	3562	3	B
13:31:30	−34:58:00	14 930	3564	3	I
13:33:48	−33:43:00	3 268	3565	-	N
13:36:06	−35:18:00	15 469	3566	4	II
13:39:24	−26:01:00	32 048	1771	-	N
13:43:54	−37:40:00	11 152	3570	-	N
13:44:36	−32:37:00	11 730	3571	2	I
13:45:18	−33:08:00	12 142	3572	-	N
13:46:18	−30:03:00	4 227	3574	-	N
13:49:42	−32:38:00	11 242	3575	4	II
13:51:30	−27:36:00	14 870	3577	4	II
13:54:42	−24:29:00	11 152	3578	3	II

References: I: Quintana et al. (1995, Paper I); II: Quintana et al. (1997, Paper II); N: NASA/IPAC, Extragalactic Database (NED; B: Bardelli et al. (1998)

structures in the region. The cluster is part of a much larger structure than was apparent from the previous observations, extending uniformly in two sheets over the whole region we surveyed to the south of the core of the SSC. We detected an additional 230 members of the SSC in our whole survey area, representing a 50% increase on the previous total of 492 SSC galaxies. Our measurements to the north of the cluster were much less complete (only one field in poor weather) so we cannot exclude the possibility that these sheets of galaxies extend equally to the north. Recent results presented by Bardelli, Zucca & Zamorani (1999) support this possibility: they have measured galaxies in 18 small (40 arcmin) inter-cluster fields north of the core of the SSC and also find an overdensity at the SSC velocity.

In Paper I the effect of the SSC on the dynamics of the Local Group was estimated. It was found that the mass in the cluster could account for at least 25% of the motion of the Local Group with respect to the cosmic microwave background. Our new data suggest that the SSC is at least 50% more massive, with a significant part of the extra mass in the closer subregion. The SSC therefore has a more important effect on the Local Group than previously thought, although we defer a detailed calculation until we have additional data (Proust et al. 1999, in preparation).

References

Bardelli, S., Zucca, E., Malizia, A., Zamorani, G., Scaramella, R., & Vettolani, G. 1996, A&A, 305, 435

Bardelli, S., Zucca, E., Zamorani, G., Vettolani, G., & Scaramella, R. 1998, MNRAS, 296, 599

Bardelli, S., Zucca, E., & Zamorani, G. 1999, in Observational Cosmology: The Development of Galaxy Systems, Sesto 1998 (astro-ph/9811015)

Drinkwater, M. J., Currie, M. J., Young, C. K., Hardy, E., & Yearsley, J. M. 1996, MNRAS, 279, 595

Infante, L., Slezak, E., & Quintana, H. 1996, A&A, 315, 657

Kraan-Korteweg, R. C., Woudt, P. A., Cayatte, V., Fairall, A. P., Balkowski, C., & Henning, P. A. 1996, Nature, 379, 519

Kurtz, M. J., & Mink, D. J. 1998, PASP, 110, 934

Metcalfe, N., Shanks, T., Fong, R., & Jones, L. R. 1991, MNRAS, 249, 498

Parker, Q. A., & Watson, F. G. 1995, in Wide Field Spectroscopy and the Distant Universe, 35th Herstmonceux Conference, ed. S. J. Maddox & A. Aragon-Salamanca (Singapore: World Scientific), p. 33

Parker, Q. A. 1997, in Wide Field Spectroscopy, 2nd Conference of the Working Group of IAU Commission 9 on Wide Field Imaging, ed. E. Kontizas et al. (Dordrecht: Kluwer), p. 25

Pierre, M., Bohringer, H., Ebeling, H., Voges, W., Schuecker, P., Cruddace, R., & MacGillivray, H. 1994, A&A, 290, 725

Quintana, H., Ramirez, A., Melnick, J., Raychaudhury, S., & Slezak, E. 1995, AJ, 110, 463 (Paper I)

Quintana, H., Melnick, J., Proust, D., & Infante, L. 1997, A&A Suppl, 125, 247 (Paper II)

Raychaudhury, S. 1989, Nature, 342, 251

Scaramella, R., Baiesi-Pillastrini, G, Chincarini, G., Vettolani, G., & Zamorani, G. 1989, Nature, 338, 562

Tody, D. 1993, in Astronomical Data Analysis Software and Systems II, ASP Conf. Ser., Vol. 52, ed. R. J. Hanisch et al. (San Francisco: PASP), p. 173

Tonry, J., & Davis, M. 1979, AJ, 84, 1511